Research Article GU J Sci 34(4): 1163-1177 (2021) DOI: 10.35378/gujs.769726

Gazi University

Journal of Science

http://dergipark.gov.tr/gujs

A Terahertz Metamaterial Absorber-Based Temperature Sensor Having Nine Resonance Peaks

Fulya BAGCI*

Ankara University, Department of Physics Engineering, 06100, Besevler, Ankara, Turkey

Highlights

- Nine-band tunable metamaterial absorber for temperature sensing applications at THz frequencies.
- Polarization-insensitive and wide-angle characteristics for two orthogonal modes.
- Broad frequency tuning range, up to 71.5%, within 40 K change of external temperature.
- Good linearity against temperature change.
- Maximum sensitivity of 11.5 GHz/K.

Article Info

Received:14 July 2020
Accepted:18 Feb 2021

Keywords

Tunable metamaterial
Polarization-insensitive
Absorption ratio
Terahertz frequency
Temperature sensing

Abstract

Design and investigation of a polarization-insensitive nine-band tunable metamaterial absorber at THz frequencies with equal to or more than 90% absorption ratio in all of the bands are reported. The tunable metamaterial absorber consists of four isosceles triangle patches with four U-shaped cut paths on top of an indium antimonide substrate, which has a fully metallic ground plane at the backside. Numerical analyses show that the metamaterial absorber has wide-angle characteristics under transverse-electric and transverse-magnetic modes. The permittivity of indium antimonide is highly dependent on temperature variations due to its temperature-dependent intrinsic carrier density, leading to shift of nine absorption peak frequencies upon change of environment temperature. Broadband switching of nine absorption peak frequencies with maximum 71.5% shift ratio between 190 K and 230 K is obtained. Temperature sensing performance of the metamaterial absorber is further evaluated and the sensitivities are found to be 11.5 GHz/K, 9.2 GHz/K, 8.3 GHz/K, 7.6 GHz/K, 7.0 GHz/K, 6.2 GHz/K, 5.3 GHz/K, 4.5 GHz/K and 4.2 GHz/K, from the first to ninth absorption band, respectively. Therefore, the proposed nine-band metamaterial absorber sensor has great potential in sensitive and accurate temperature measurement, absorption tuning in optoelectronic applications and as frequency selective thermal emitters.

1. INTRODUCTION

A great deal of attention has been devoted to research upon metamaterial absorbers over the last decade. In principle, the concept of high impedance surfaces used for eliminating the propagation of surface waves in antennas [1-2] paved the way for the development of perfect metamaterial absorbers. However, it was Landy et al. [3] who gave stimulus to metamaterial absorber (MA) research in 2008 with their MA, which has compact feature as well as more than 85% absorption performance. Although preliminary works based on MAs were mainly related to radio and microwave frequencies [4], achievements both in manufacturing processes of metamaterials and experimental techniques, such as generation of THz sources, time-domain spectroscopic techniques, allowed the realization of MAs also in the terahertz and optical frequency regimes [5-10]. Extension of the frequency scale has permitted substantial increase in the application areas of MAs for emerging potential applications in spectroscopy, sensing and imaging.

One of the constrictions related to perfect absorption based on metamaterials is the narrow absorption bandwidth due to the resonant nature of these materials. Many design techniques are proposed to operate MAs at multiple frequencies. One straightforward technique relies on stacking layers that possess resonant overlapping absorption modes at multiple-frequencies [11-12]. Ding et al. [11] used twenty metal-dielectric

* e-mail: Fulya.Bagci@eng.ankara.edu.tr

multi-layered pyramids on top of a ground layer and Zhu et al. [12] stacked five gradually modified square metallic patches to merge the resonance bands. However, when the number of layers is increased, it becomes difficult to precisely align the layers in the fabrication process. Another straightforward technology to operate MAs at multiple frequencies can be regarded as employing concentric ring resonators in the unit cell, such as nested closed square rings or split-ring resonators [9,13,14]. In this method, the number of rings basically determines the number of absorption bands [9,13,14]. Alternative metallic or complementary inclusions are also added to well-known resonator structures to simply increase the frequencies of operation [15-16].

Electromagnetic properties of the multi-band MAs are usually fixed after the design and fabrication process. Therefore, dynamic tuning of the absorption frequencies is highly demanding to achieve reconfigurable and tunable devices. Dynamically controllable MA for THz frequencies is firstly demonstrated via photoexcitation [17] and voltage control [18] of free carries in a semiconductor GaAs substrate. Subsequently, high temperature superconductive films are proposed for resonance tuning [19-21]. The imaginary part of the conductivity of high temperature superconductive films is very sensitive to external stimulations so that the tuning can be realized by changing the temperature [19-20], applying magnetic fields [19,21] and varying photoexcitation fluence [22-23]. However, the necessary temperature and pressure environments for these absorbers put a restriction on their practical use. Microwave MAs based on voltage controlled varactor diodes through vias and bias lines [24-25] and THz MAs based on electrostatically activated micro-electro-mechanical systems cantilever and split ring resonators [26] have also been proposed. These methods do not offer relevant results for vast production, since the fabrication process of absorbers hosting vias, lumped elements, cantilevers, etc. is not straightforward.

Recently, there has been extensive research on tunable MAs by combining the resonators with graphene [27-32], microfluidics [33] and liquid crystals [34-35]. However, there are a number of challenges for these tunable MA approaches. As for the graphene, the production of single or multiple-patterned graphene layers is cumbersome and device fabrication is hard to be accomplished. Microfluidic tunable MAs require the deployment of capillary channels for the flow of fluidic materials, as well as a rapid change of the fluidic material to tune the absorption frequency. Liquid-crystal devices are highly promising as terahertz components, however the tunability range is usually limited. For example, modulation of the reflectance is accomplished by shifting the resonance less than 20% in frequency [35]. On the other hand, temperature modulation method offers superior advantages, such as wide-range tunability and ability to integrate with electric or thermal modules for device application [36].

Temperature is changed conveniently by varying the electric current in the interdigital electrodes [37] and in the micro-fabricated electric heating wires [10]. A shift in the passband frequency of a single-band MA-loaded ferroelectric barium strontium titanate film from 0.826 THz to 0.905 THz under a temperature change from 25 °C to 105 °C is obtained [10]. A phase-change material, VO_2 film, is introduced between two silica spacers to tune the peak absorption frequencies of the MA from 30% to 100% [38]. Temperature-dependent strontium titanate and vanadium dioxide are proposed to shift the resonance frequency of single and dual-band MAs, respectively [39]. A frequency-tuning range as large as 80.4% within the temperature range of 40 K is achieved by employing indium antimonide (InSb) as the dielectric substrate [40]. However, the proposed MA has resonance only at a single frequency [40]. The number of absorption bands is achieved to be six with metallic cross-cave-patch MA structure on InSb substrate and maximum 55.3% frequency-shift is obtained between 190 K and 230 K [41]. Towards the end of 2020, a temperature tunable MA on InSb substrate having eight absorption resonance bands is reported [42]. The resonator pattern on top of the 16 μm-thick InSb substrate included four triangular tapered structures connected by a circular ring [42]. Improving the resonator pattern of [41] and using only a 9.0 μm-thick InSb dielectric spacer, in this study the number of absorption bands is increased to nine and maximum frequency tuning range is achieved to be 71.5%. In addition, the dependence of absorption performance on the angle of incidence is also investigated in detail for transverse-electric (TE) and transverse-magnetic (TM) polarizations. A robust absorption performance against temperature change is observed.

In this work, a nine-band THz metamaterial absorber with gold resonators on top of a ground-backed InSb dielectric layer is proposed. The proposed nine-band MA has high levels of absorption, exceeding 89% for

all the bands. In addition, it does not suffer from change in the polarization angle. Absorption mechanism is revealed by analyzing the electric field distributions at resonance frequencies. The absorption peak frequencies are able to be tuned in the frequency range of 71.5%, 40.7%, 31.5%, 26.4%, 21.7%, 16.3%, 11.5%, 8.0% and 7.1%, respectively, from the lowest to highest resonance frequency upon the change of temperature from 190 K to 230 K.

2. MATERIAL AND METHOD

The metamaterial absorber is composed of two metallic layers, namely, top resonator-layer and ground-plane, separated by an InSb substrate. The schematic front-view of the unit cell of the MA is displayed in Figure 1 with its geometric parameters. The top layer consists of four isosceles triangle patches in which four intertwined tracks are carved inward to increase the number of absorption bands with high absorption efficiency. The optimized geometric parameters for nine-band absorption are determined as (dimensions in μm): w_1=2.0, w_2=11.5, g_1=1.5, g_2=10.9, g_3=4.5, g_4=4.5, l_1=83.6, l_2=56.0 and l_3=24.5. The periodicity, p, is 105 μm in $\pm x$ and $\pm y$ directions.

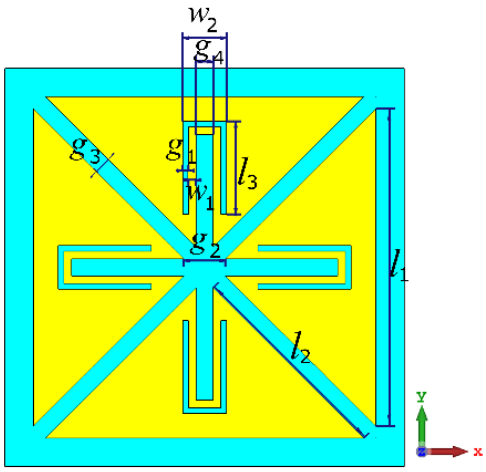

Figure 1. *Schematic front face view of the MA unit cell*

Resonators on the top of the substrate and the ground layer are made of gold with a conductivity of σ=4.09×10^7 S/m, which is a good approximation in the operation frequency range of 0.5-2.5 THz [41,42]. The MA is designed to possess four-fold symmetry to have polarization independent character. InSb is chosen as the dielectric layer due to its large electron mobility and small energy gap. The thickness of the substrate layer and gold metallic layer are 9.0 μm and 0.4 μm, respectively. InSb is modelled with a temperature-dependent Drude-like permittivity function, which is defined as [40-42]:

$$\varepsilon(\omega) = \varepsilon_\infty - \frac{\omega_p^2}{\omega^2 + i\gamma\omega} \quad . \tag{1}$$

In Equation (1), ε_∞ stands for the high frequency bulk permittivity, which is equal to 15.68. γ refers to the damping constant and ω_p is the plasma frequency [40-42].

The plasma frequency is expressed as $\omega_p = \sqrt{Ne^2 / \varepsilon_0 m^*}$, which is related to the intrinsic carrier density (N), charge of one electron (e), permittivity of free space (ε_0) and effective mass of the free carriers (m^* =0.015m_e) [40-42]. Damping constant (γ) depends on the electron mobility μ, given by $\gamma = e/(m^*\mu)$ [40-42]. Since electron mobility remains almost constant between 190 K and 230 K in the frequency range of 0.5 THz to 2.5 THz, the damping constant is accepted to be constant and equal to $\gamma = 0.1\pi$ THz [41,42]. On the other hand, the intrinsic carrier density N (in m^{-3}) of InSb is highly dependent on the temperature T as given by the formula [40-43]:

$$N = 5.76\times10^{20} T^{1.5} \exp(-0.13 / k_B T) \, . \tag{2}$$

In Equation (2), k_B is the Boltzmann constant in eV.K^{-1} and T is the temperature in K.

As the temperature rises, the intrinsic carrier density (N) increases. Thus, the semiconducting feature of the InSb changes to metallic feature, leading to an increase in the plasma frequency. According to Equation (1), the change of the plasma frequency will alter the real and imaginary parts of the permittivity of InSb. Therefore, external changes in the temperature will eventually affect the resonance properties of the proposed MA.

Absorption is defined as $A=1-|S_{11}|^2-|S_{21}|^2$, where A is absorption, $|S_{11}|$ and $|S_{21}|$ are the magnitudes of reflection and transmission coefficients, respectively. Since the ground is covered with the gold metallic plate, $|S_{21}|^2\approx0$, so absorption can be readily calculated as $A=1-|S_{11}|^2$. Absorption spectra and field distributions are calculated by using CST Microwave Studio (MWS), which employs finite-integration technique. Along the four sides of the unit cell, unit cell boundaries are used in CST MWS, whereas open space region is utilized in the direction of wave propagation. Electromagnetic waves are sent through normal direction to the structure, with the E-field vector in x and H-field vector in y directions.

3. RESULTS AND DISCUSSIONS

3.1. Polarization-Insensitive Multi-Band Absorption Behavior of the Metamaterial Absorber

Absorption spectrum of the proposed metamaterial absorber at T=190 K is shown in Figure 2(a). It is noteworthy to mention that the frequency range of the absorption spectrum is not exceeded more than 2.5 THz in order to exclude higher-order modes. There exists nine absorption peaks with equal or more than 90% absorption ratio. Absorption selectivity of the nine resonance peaks is analyzed by defining an absorption extinction ratio parameter, which can be calculated from the ratio of peak absorption ratio to the minimum absorption ratio outside resonance at the lower or upper-frequency surroundings of the band. The information of mode number, resonance frequencies (f_0), peak absorption ratios, full-width at half-maximum (FWHM) bandwidths, quality factors (Q-factors) and absorption extinction ratios are presented in Table 1. Absorption extinction ratio is high except the third, fourth and eight resonance bands, indicating a good frequency selectivity for the presented MA. Good impedance matching with free space is a prerequisite for a high absorption peak. For perfect absorption, the real part of the impedance of the MA should be very close to the input impedance of free space, which is 377 Ω, whereas the imaginary part of the impedance should almost be equal to zero. It is noticeable from Table 1 that especially the mode numbers 2, 5, 7, 8, and 9 have more than 95% absorption, which means that a very good impedance matching is realized for these modes. The values of the Q-factors are found to be comparable to [41] and greater than those reported in [44] indicating a strong potential applicability to be used in sensing or detecting. Furthermore, absorption performance of the presented MA is insensitive to incoming electromagnetic waves from any polarization direction as demonstrated in Figure 2(b).

Table 1. *Resonance frequency, absorption peak (%), FWHM bandwidth, Q-factor and absorption extinction ratio values for the nine resonance modes*

Mode number	1	2	3	4	5	6	7	8	9
Resonance frequency, (THz)	0.64	0.91	1.05	1.14	1.29	1.47	1.79	2.20	2.29
Absorption peak (%)	89.50	95.83	89.85	92.37	99.59	93.03	99.90	97.43	99.87
FWHM bandwidth (THz)	0.027	0.038	0.043	0.040	0.029	0.032	0.055	0.105	0.043
Q-factor	15.72	17.68	23.95	23.84	34.40	51.57	30.67	20.95	53.02
Absorption extinction ratio	54.94	15.00	3.38	5.34	12.39	21.14	22.70	6.50	8.78

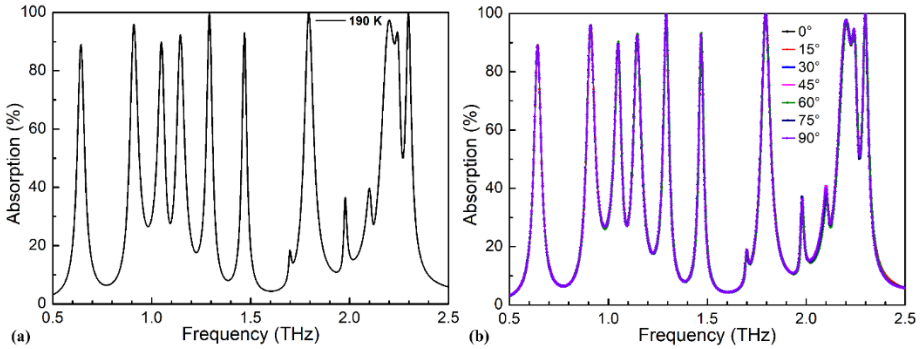

Figure 2. *Absorption spectra of the MA a) for normal direction and b) for different polarization angles at T=190 K*

In order to reveal the relationship between the electric field distributions and the MA structure, electric field distributions on the front face of the MA are analyzed at the nine resonance peaks and the results are illustrated in Figure 3(a-i). The electric field vector of the impinging electromagnetic waves is arbitrarily kept in parallel to the *y*-axis for this analysis. As shown in Figure 3(a), at the first (lowest) resonance frequency at 0.64 THz, the electric field is concentrated at the edges of the top and bottom triangular patches with a node at top and bottom sides. However, the electric field is localized at the left and right patches and at U-shaped slots for the second resonance frequency at 0.91 THz (Figure 3(b)). Besides, for the third resonance frequency at 1.05 THz, the electric field is also concentrated at the left and right U-shaped slots as well as at the three corners of the top and bottom triangular patches (Figure 3(c)). Similarly, the electric field concentrates on the same areas but with higher strength for the fourth resonance at 1.14 THz, as shown in Figure 3(d). In the adjacent figure, Figure 3(e), at 1.29 THz, electric field tends to be localized at the edges of left and right triangular patches in addition to left and right U-shaped slots. When it comes to the sixth resonance at 1.47 THz, as it can be seen in Figure 3(f), four nodes appear at the edges of the left and right triangular patches. In addition, one node is prominent at the left and right U-shaped slots. Besides, as seen in Figure 3(g), for the seventh resonance at 1.79 THz, five nodes are clearly visible at the edges of the triangular patches and one node at the top and bottom U-shaped slots. The complexity of the node pattern in the electric field distribution increases for the eighth resonance at 2.20 THz, as it is noticeable from Figure 3(h). Although there is weak electric field localization at the edges of the triangular patches, the main confinement is at the top and bottom U-shaped slots, similar to Figure 3(g). Lastly, for the ninth resonance at 2.30 THz, electric field localization is more distributed as seen in Figure 3(i). However, it is mostly localized at the top and bottom U-shaped slots and at the corners of the left and right triangular patches at the unit cell center.

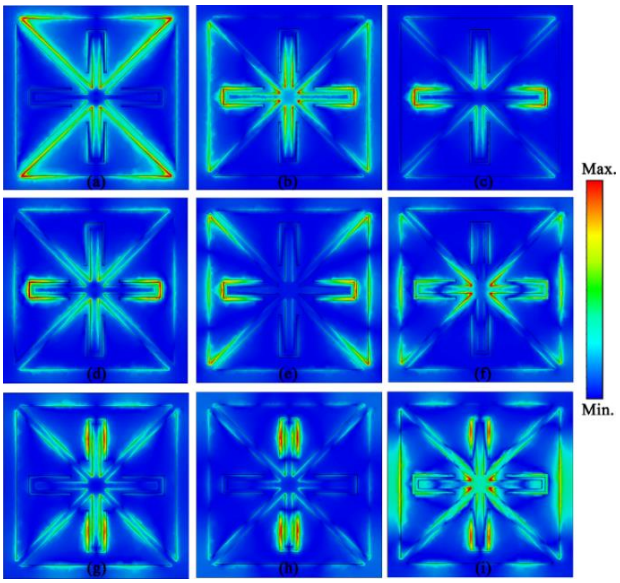

Figure 3. *Electric field distributions on the front face of the MA at normal direction for the a) first, b) second, c) third, d) fourth, e) fifth, f) sixth, g) seventh, h) eighth and i) ninth resonance at T=190 K*

3.2. Effect of Incident Angle on the Absorption Performance of the Metamaterial Absorber

Influence of incident angle on absorption performance is examined when the incident angle is varied between 0° and 60°. Figure 4(a) displays the corresponding absorption spectra in 20° increment steps of incident angle for TE polarization, in which the electric field vector is always parallel to the metamaterial surface. When the incident angle is 20°, the first eight absorption bands maintain their peak frequency, whereas the ninth absorption band shifts to higher frequency at 2.4 THz. The peak absorption ratios only change for the first and third absorption bands from 89% to 85.5% and from 89.7% to 83.7%, respectively. A new absorption band with 47.0% absorption becomes prominent between the sixth and seventh absorption bands when θ=40°. Peak absorption ratios at resonances decrease slightly more, except the fifth absorption band, whereas the eighth absorption band splits to three shoulders. Peak absorption ratio continues to decrease when θ is 60° but the average of peak absorption ratio of the nine bands is still greater than 70%.

Color plot of the absorption spectra are depicted in Figure 4(b) for TE polarization. Here calculated step of incident angle is set to be 1°. It is evident that absorption ratios maintain at high values for large oblique incidence. In addition, absorption bandwidth is stable for the second, fourth, fifth and sixth absorption bands. Absorption is attenuated at some extent for large oblique incidence as it becomes more difficult to excite the triangular patches and U-shaped slots.

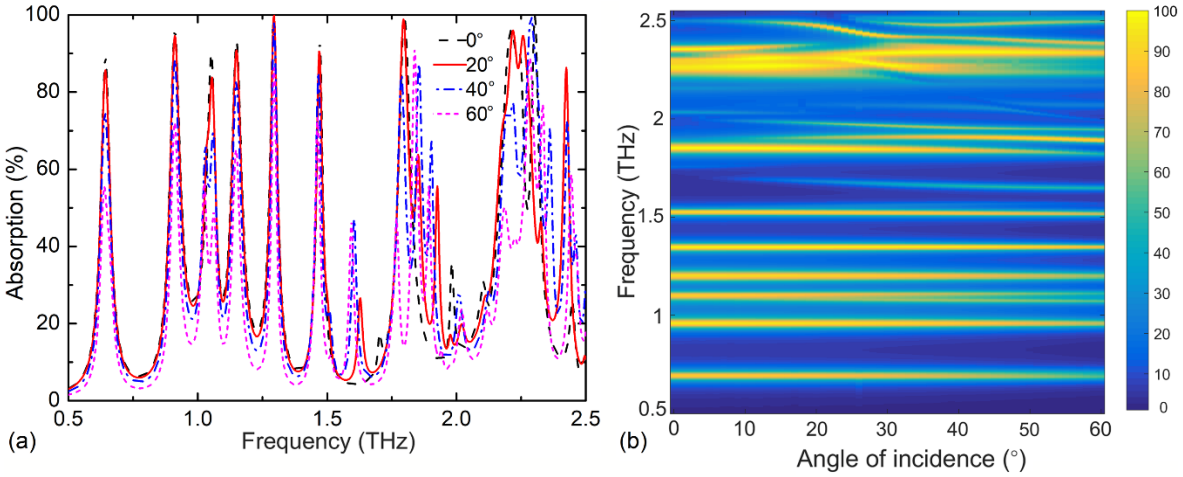

Figure 4. *a) Absorption spectra at different incident angles and b) color plot of frequency versus incident angle under TE-mode excitation at T=190 K*

Absorption spectra under TM-mode excitation, where the direction of the electric field vector changes as the direction of propagation vector alters, are depicted in Figure 5(a) for θ=0° and 20° and in Figure 5(b) for θ=40° and 60°. When the incident angle is increased to 20°, new absorption bands emerge since metallic patches are very sensitive to the change in the direction of the electric field vector. A new absorption band appears between the fourth and fifth absorption bands at 1.236 THz with 83.5% absorption, as well as two for each absorption bands are pronounced with moderate absorption ratios (74.3%, 60.1%, 56.1%, 68.5%) between the sixth and seventh and seventh and eighth absorption bands. In addition, a new shoulder with 90.0% absorption arises next to the ninth absorption band. In brief, the number of absorption bands increases to fifteen for θ=20°. The prior nine bands, which occur at normal incidence, maintain their absorption peak frequency and ratio when θ=20°. However, when the incidence angle is 40°, the third, fourth and fifth absorption bands for θ=20° merge to have 0.21 THz FWHM bandwidth and the absorption ratio for the fifth shoulder reaches 99.8%. In addition, absorption ratio of the eighth, ninth and thirteenth bands increase to be 99.8%, 60.2% and 97.6%, respectively. There is a noticeable decrease in the absorption ratio for the last three absorption bands (thirteenth, fourteenth and fifteenth) for θ=40°. However, these bands increase to have more than 85% peak absorption and merge to create a wide band when θ=60°. Moreover, the amplitudes of the eleventh and twelfth absorption bands rise to possess 95.4% and 87.5% peak absorption ratios, respectively, when θ=60°. Absorption ratios of almost all of the absorption bands except the seventh band at 1.49 THz improve when the oblique incidence is 60°. Absorption spectra are

also calculated under TM-mode excitation for oblique incidences in the interval of 1° and the results are presented in Figure 6 with color plot. It is obvious from Figure 6 that in the high frequency range new absorption bands with high absorption ratios emerge as the incidence angle of the electromagnetic waves increases.

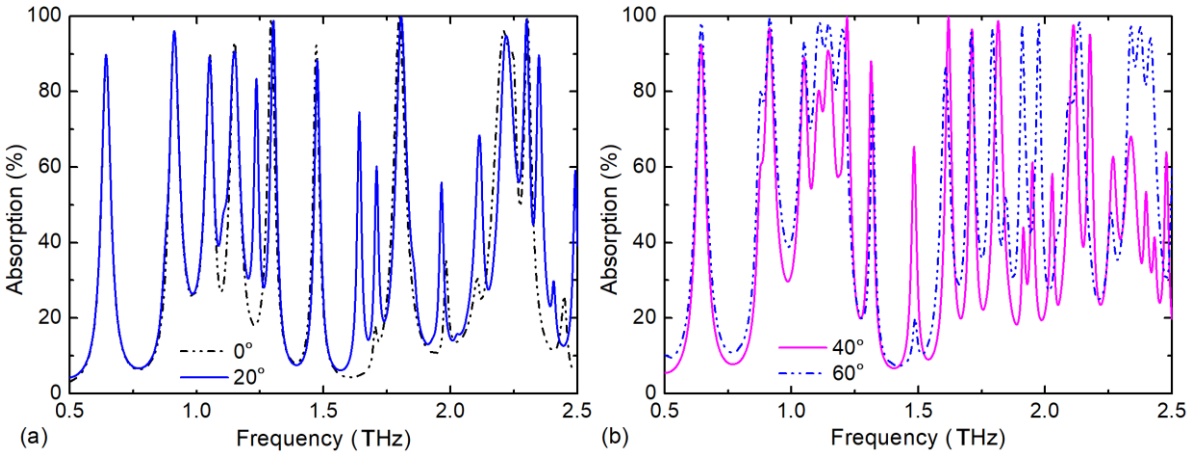

Figure 5. *Absorption spectra at different incident angles under TM-mode excitation at T=190 K: a) θ=0° and θ=20° and b) θ=40° and θ=60°*

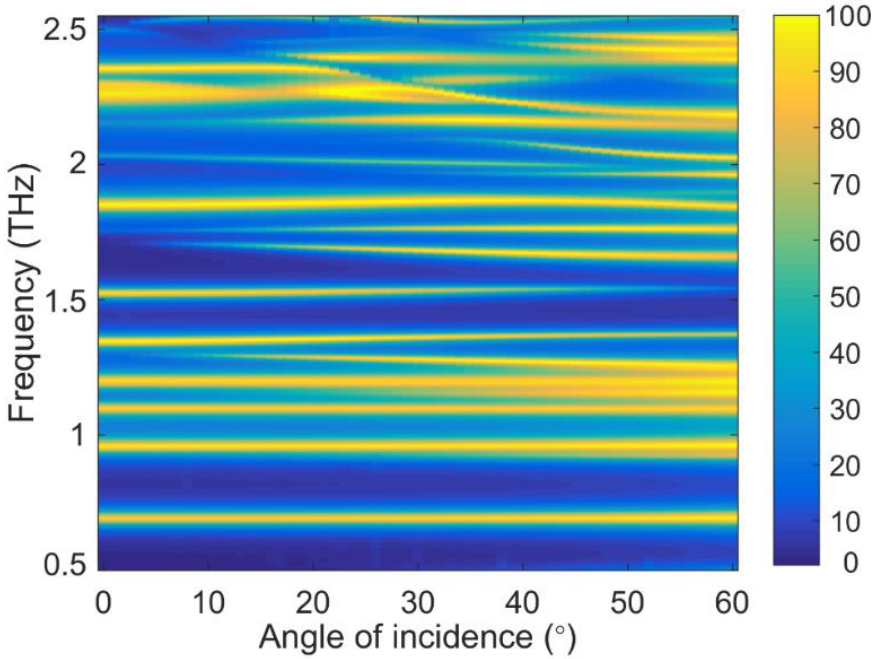

Figure 6. *Color plot of frequency versus incident angle under TM-mode excitation at T=190 K*

Any mismatches in the dimensions of the geometric parameters due to fabrication imperfections may affect the performance of the MA. In order to analyze this issue, absorption spectra are first calculated under slight variations in the periodicity of the MA. Figure 7 shows the absorption spectra of the MA under ±5 μm deviations in the unit cell periodicity. It is apparent from Table 2 that the resonance frequencies of the first (lowest frequency) four resonances and the seventh as well as the ninth resonance are not affected at all from the change in periodicity. The resonance frequency of the fifth mode decreases as the periodicity increases. Absorption peak ratios of the first four bands and the eighth band decrease as the periodicity is increased, whereas the absorption peak ratio of the sixth band increases. The *Q*-factor increases for the first five resonance bands slightly and for the ninth resonance band remarkably, but it decreases for the sixth, seven and eighth resonance bands. On the whole, the variations in the resonance frequency, absorption peak ratio and *Q*-factor are in a low degree so that the performance of the nine-band MA is maintained.

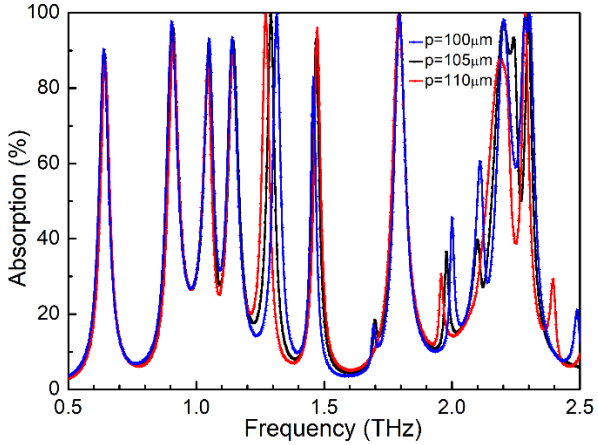

Figure 7. *Absorption spectra at T=190 K under slight variations in the periodicity (p) of the MA*

Table 2. *Resonance frequency, absorption peak (%), and Q-factor values for the nine resonance modes under slight variation of the periodicity from p=105 μm*

	1.mode	2.mode	3.mode	4.mode	5.mode	6.mode	7.mode	8.mode	9.mode
Res. freq. (THz), *p*=100 μm	0.64	0.90	1.05	1.14	1.31	1.46	1.79	2.20	2.28
Res. freq. (THz), *p*=110 μm	0.64	0.91	1.05	1.14	1.27	1.47	1.79	2.20	2.28
Abs. peak (%), *p*=100 μm	90.3	97.6	93.1	93.5	99.7	82.8	99.2	98.1	98.6
Abs. peak (%), *p*=100 μm	87.2	93.4	86.1	88.8	99.7	95.9	99.2	87.8	99.8
Q-factor, *p*=100 μm	15.58	16.88	22.02	22.80	34.47	66.66	33.40	27.23	29.23
Q-factor, *p*=110 μm	16.50	18.35	25.73	24.78	34.70	45.94	28.41	22.27	57.00

The effects of possible deviations in the fine details of the geometrical structure, such as w_1 and g_1 of the carved intertwined tracks, during the fabrication process are also investigated. The resonance band characteristics for different w_1 parameters are illustrated in Figure 8(a) and the resonance frequency, absorption peak ratio and *Q*-factor for the nine resonance modes are tabulated in Table 3. Resonance characteristics of the first, fifth and ninth resonance band do not alter from w_1 variation. On the other hand, resonance frequencies of the second and seventh band decrease as w_1 increases. Absorption peak ratio of the second resonance band decreases, whereas that of the third, fourth and eighth bands increase as w_1 is increased. Specifically, in order to increase the peak absorption ratio of the third band more than 76%, w_1 should be increased more than 1.5 μm. However, the *Q*-factor of the third band decreases by 36.6% as w_1 is changed from 1.5 μm to 2.5 μm. The increase of w_1 to 2.5 μm widens the eighth band and decreases the *Q*-factor of this band.

Table 3. *Resonance frequency, absorption peak (%), and Q-factor values for the nine resonance modes under slight variation of w_1 from w_1=2.0 μm*

	1.mode	2.mode	3.mode	4.mode	5.mode	6.mode	7.mode	8.mode	9.mode
Res. freq.(THz), w_1=1.5 μm	0.64	0.88	1.05	1.16	1.29	1.48	1.81	2.22	2.30
Res. freq.(THz), w_1=2.5 μm	0.64	0.89	1.04	1.13	1.29	1.45	1.77	2.17	2.29
Abs. peak (%), w_1=1.5 μm	89.6	99.6	75.6	87.3	99.2	93.3	98.9	94.1	99.9
Abs. peak (%), w_1=2.5 μm	88.1	88.4	94.5	94.9	99.6	92.8	99.5	99.2	99.7
Q-factor, w_1=1.5 μm	15.72	16.40	33.49	24.06	33.86	53.05	30.53	22.05	48.85
Q-factor, w_1=2.5 μm	15.88	19.56	21.22	22.64	35.83	48.66	31.55	16.58	49.46

Since the width of the U-shaped slots for the optimized MA is 2.0 μm, the effect of any deviations in the fabrication process to resonance characteristics is also analyzed. The absorption spectra related to g_1=1.0 μm, 1.5 μm and 2.0 μm are plotted in Figure 8(b) and the resonance frequency, absorption peak ratio and *Q*-factor for the nine resonance bands are listed in Table 4. The resonance frequencies of only the second and seventh resonance bands are notably affected from the change of g_1. For the related bands, the resonance frequencies decrease as g_1 is increased. Especially, the absorption peak ratio of the third and fourth

resonance bands can be increased by increasing the parameter g_1 at the cost of slight decrease of the absorption peak ratio for the first, second and eighth resonance bands. As for the *Q*-factors, *Q*-factors of the first, second, fifth, sixth and seventh bands slightly increase, whereas those for the third, fourth and ninth bands decrease as g_1 is increased. Therefore, the analyses of the MA for temperature sensing applications are continued with the aforementioned structural parameters mentioned in section 2.

Table 4. *Resonance frequency, absorption peak (%), and Q-factor values for the nine resonance modes under slight variation of g_1 from g_1=1.5 μm*

	1.mode	2.mode	3.mode	4.mode	5.mode	6.mode	7.mode	8.mode	9.mode
Res. freq. (THz), g_1=1.0 μm	0.64	0.93	1.05	1.15	1.29	1.48	1.81	2.21	2.29
Res. freq. (THz), g_1=2.0 μm	0.64	0.90	1.05	1.15	1.29	1.46	1.78	2.20	2.30
Abs. peak (%), g_1=1.0 μm	90.0	98.4	79.0	82.5	99.2	92.7	99.7	99.6	99.6
Abs. peak (%), g_1=2.0 μm	87.7	92.8	94.2	97.2	99.6	93.0	99.8	95.2	98.8
Q factor, g_1=1.0 μm	15.67	15.47	27.63	25.00	33.08	49.50	28.28	19.39	50.89
Q factor, g_1=2.0 μm	16.41	19.82	22.97	22.68	35.44	50.87	32.26	19.91	46.94

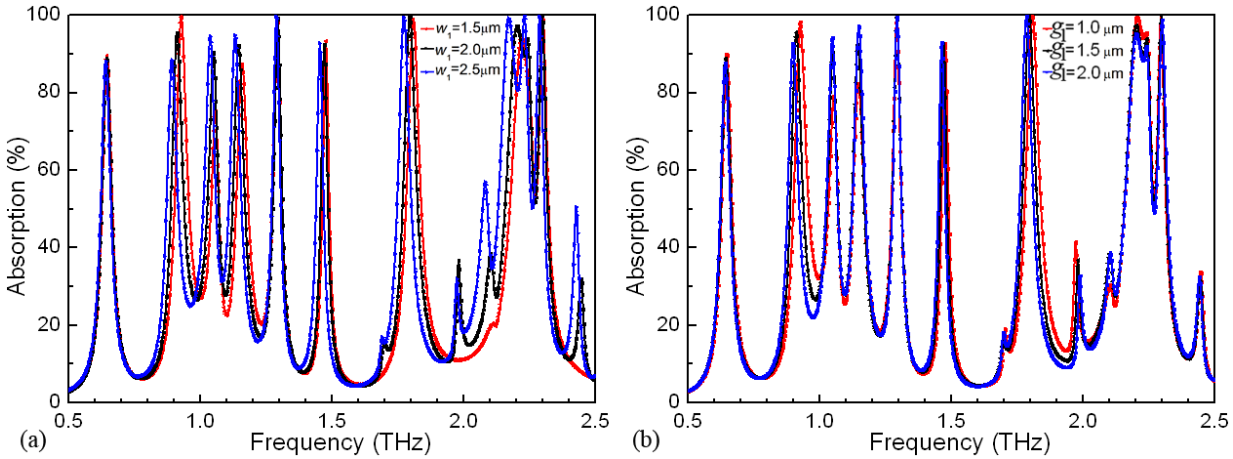

Figure 8. *Absorption spectra at T=190 K under slight variations in the a) w_1 parameter and b) g_1 parameter of the MA*

3.3. Temperature Sensing Performance of the Metamaterial Absorber

Permittivity of InSb is delicate to external temperature of the ambient so that it can be used for active tuning of absorption resonance by changing the temperature. Absorption spectra of the MA under different ambient temperatures are calculated and the results for *T*=190 K, *T*=200 K, *T*=210 K, *T*=220 K and *T*=230 K are illustrated in Figure 9(a)-(e), respectively. It can be seen at first glance that the peak absorption ratios do not show any decrease for temperatures other than 190 K except the fifth absorption band. This shows that the highly absorptive behavior of the nine band MA design is very robust against any temperature change. This is due to the fact that the loss tangent of InSb is not very sensitive to external temperature variation. When the temperature is varied between 190 K and 230 K, all the nine resonances shift to higher frequencies. The amount of shift in the absorption resonance frequency (Δf) upon change of temperature is listed in the first line of Table 5. If the shifting of first six bands of our proposed MA is compared with the six-band InSb MA [41], it can be observed that the shifting amount of our proposed MA is approximately 0.05 THz greater for all the bands within the 190 K to 230 K interval. The range of frequency shifting is also evaluated in percentage form from $\Delta f/f_0$ and listed in the second line of Table 5. From these results, it can be deduced that the presented MA can be used as a temperature sensor in spectroscopic applications.

Table 5. *Shifting amount of the nine resonance peaks in the temperature interval of 190 K to 230 K*

ΔT: 190-230 K	1st resonance	2nd resonance	3rd resonance	4th resonance	5th resonance	6th resonance	7th resonance	8th resonance	9th resonance
Δf	0.46 THz	0.37 THz	0.33 THz	0.30 THz	0.28 THz	0.24 THz	0.21 THz	0.18 THz	0.16 THz
$\Delta f/f_0$	71.5%	40.7%	31.5%	26.4%	21.7%	16.3%	11.5%	8.0%	7.1%

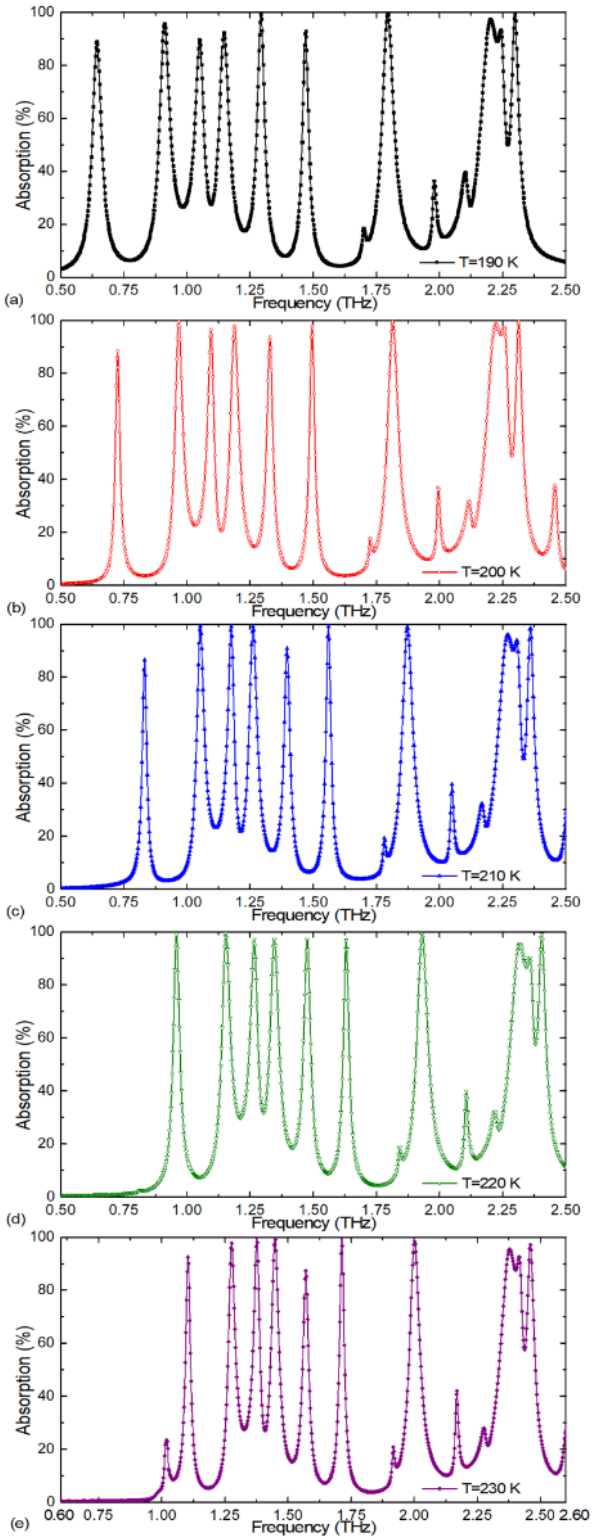

Figure 9. *Absorption spectra of the MA under various temperatures: a) 190 K, b) 200 K, c) 210 K, d) 220 K and e) 230 K*

It is important to indicate a sensitivity parameter to facilitate comparison of the ambient temperature sensing performance of the proposed MA. Conventionally, the sensitivity (S) of a temperature sensor is defined as the ratio of the shift of frequency (Δf) to the variation in temperature (ΔK): $S=\Delta f/\Delta K$. The shifts of resonance frequency for different temperatures of the surrounding ambient between 190 K and 230 K are shown in Figure 10(a-c) for the nine absorption bands. The shift, as shown in Figure 10, shows a linear variation with the change of the temperature of the environment. The slope of the fitted line gives the S parameter values for the nine absorption bands. The obtained S parameters are listed in Table 6 for the nine resonances. It is clear that the sensitivity values and the number of absorption bands of the cross-cave-patch [41] are enhanced by carving four intertwined tracks inside of the four triangular patches and optimizing the geometry.

Table 6. *Sensitivity of the nine resonance peaks in the temperature interval of 190 K to 230 K*

ΔT: 190-230 K	1st resonance	2nd resonance	3rd resonance	4th resonance	5th resonance	6th resonance	7th resonance	8th resonance	9th resonance
Sensitivity (GHz/K)	11.5	9.2	8.3	7.6	7.0	6.2	5.3	4.5	4.2

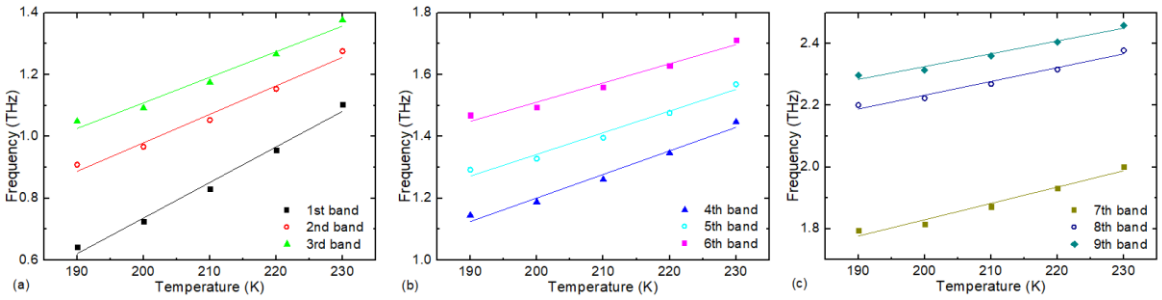

Figure 10. *Absorption peak frequency versus ambient temperature for the a) first, second and third band, b) fourth, fifth and sixth band and c) seventh, eighth and ninth band*

The performance of the proposed design is compared with the recent temperature-tunable terahertz metamaterial absorbers in terms of number of resonances, lowest resonance frequency, used temperature-dependent material and maximum sensitivity. The results are listed in Table 7. It is apparent from Table 7 that the maximum number of resonances of terahertz temperature-tunable metamaterial absorbers is reached to nine for the first time in the literature by this work. The sensitivity of the presented structure is greater than the sensitivity of the temperature tunable single band [39.45,46] and multi-band MAs [41-42]. Additionally, the used InSb substrate in this study is both physically and electrically thinner than that used for the seven band [47] and octa band [42] THz MA temperature sensors. Consequently, the proposed simple design MA can be employed in temperature sensing applications for better sensitivity in a wider frequency range.

Table 7. *Comparison of the performance of different temperature-tunable terahertz MAs*

Reference	Resonance number	Lowest resonance frequency	Temperature dependent material used	Max. sensitivity (GHz/K)
[39]	1	1.41 THz at 200K	strontium titanate	0.55
[40]	1	0.715 THz at 190K	indium antimonide	11.5
[45]	1	1.71 THz at 200K	strontium titanate	3.85
[46]	1	1.32 THz at 190K	indium antimonide	6.94
[41]	6	0.746 THz at 190K	indium antimonide	10.3
[47]	7	0.75 THz at 190K	indium antimonide	12.6
[42]	8	0.859 THz at 190K	indium antimonide	10.3
This work	9	0.64 THz at 190K	indium antimonide	11.5

4. CONCLUSIONS

In summary, an actively controllable nine-band polarization-insensitive metamaterial absorber with greater-equal than 90% absorption in all bands is proposed. The unit cell of the metamaterial absorber consists of four isosceles triangle gold patches with four U-shaped slots on a ground-backed InSb substrate. Electric field distributions are analyzed at resonance frequencies to get a physical insight on the resonant absorption mechanism. It is shown that the proposed metamaterial absorber keeps its high absorption characteristics for the nine bands for both TE and TM modes even at 60° angle of incidence. Moreover, the proposed metamaterial absorber keeps its superior performance under fabrication imperfections. When the temperature is altered from 190 K to 230 K, the amount of the observed shift from the lowest to highest resonance frequency are found to be 0.46 THz, 0.37 THz, 0.33 THz, 0.30 THz, 0.28 THz, 0.24 THz, 0.21 THz, 0.18 THz and 0.16 THz, respectively. Hence, the temperature sensitivity of the proposed absorber are obtained as 11.5 GHz/K, 9.2 GHz/K, 8.3 GHz/K, 7.6 GHz/K, 7.0 GHz/K, 6.2 GHz/K, 5.3 GHz/K, 4.5 GHz/K and 4.2 GHz/K for the all bands from lower to higher resonance frequency. We believe the broadband switching property of the proposed MA design will be of great benefit in temperature sensing and many optoelectronic-related applications.

CONFLICTS OF INTEREST

No conflict of interest was declared by the author.

REFERENCES

[1] Sievenpiper, D., Zhang, L., Jimenez Broas, R.F., Alexopolous, N.G., Yablonovitch, E., "High-impedance electromagnetic surfaces with a forbidden frequency band", IEEE Transactions on Microwave Theory and Techniques, 47(11): 2059–2074, (1999). DOI: 10.1109/22.798001

[2] Simovski, C.R., Maagt, P. de, Melchakova, I.V., "High-impedance surfaces having stable resonance with respect to polarization and incidence angle", IEEE Transactions on Antennas and Propagation, 53(3): 908–914, (2005). DOI: 10.1109/TAP.2004.842598

[3] Landy, N.I., Sajuyigbe, S., Mock, J.J., Smith, D.R., Padilla, W.J., "A perfect metamaterial absorber", Physical Review Letters, 100: 207402, (2008). DOI: 10.1103/PhysRevLett.100.207402

[4] Watts, C.M., Liu, X., Padilla, W.J., "Metamaterial electromagnetic wave absorbers", Advanced Materials, 24: OP98–OP120, (2012). DOI: 10.1002/adma.201200674

[5] Chen, H-T., Yang, H., Singh, R., O'Hara, J.F., Azad, A.K., Trugman, S.A., Jia, Q.X., Taylor, A.J., "Tuning the resonance in high-temperature superconducting terahertz metamaterials", Physical Review Letters, 105(24): 247402, (2010). DOI: 10.1103/PhysRevLett.105.247402

[6] Bossard, J.A., Lin, L., Yun, S., Liu, L., Werner, D.H., Mayer, T.S., "Near-ideal optical metamaterial absorbers with super-octave bandwidth", ACS Nano, 8(2): 1517–1524, (2014). DOI: 10.1021/nn4057148

[7] Liu, Z., Li, Y., Zhang, J., Huang, Y., Li, Z., Pei, J., Fang, B., Wang, X., Xiao, H., "Design and fabrication of a tunable infrared metamaterial absorber based on VO_2 films", Journal of Physics D: Applied Physics, 50: 385104, (2017). DOI: 10.1088/1361–6463/aa8338

[8] Kadlec, C., Skoromets, V., Kadlec, F., Němec, H., Chen, H.-T., Jurka, V., Hruška, K., Kužel, P., "Electric-field tuning of a planar terahertz metamaterial based on strained $SrTiO_3$ layers", Journal of Physics D: Applied Physics, 51: 054001, (2018). DOI: 10.1088/1361-6463/aaa315

[9] Shen, X., Yang, Y., Zang, Y., Gu, J., Han, J., Zhang, W., Cui, T.J., "Triple-band terahertz metamaterial absorber: Design, experiment, and physical interpretation", Applied Physics Letters, 101: 154102, (2012). DOI: 10.1063/1.4757879

[10] Dong, B., Ma, H., Wang, J., Shi, P., Li, J., Zhu, L., Lou, J., Feng, M., Qu, S., "A thermally tunable THz metamaterial frequency-selective surface based on barium strontium titanate thin film", Journal of Physics D: Applied Physics, 52: 045301, (2019). DOI: 10.1088/1361-6463/aaebef

[11] Ding, F., Cui, Y., Ge, X., Jin, Y., He, S., "Ultra-broadband microwave metamaterial absorber", Applied Physics Letters, 100: 103506, (2012). DOI: 10.1063/1.3692178

[12] Zhu, J., Ma, Z., Sun, W., Ding, F., He, Q., Zhou, L., Ma, Y., "Ultra-broadband terahertz metamaterial absorber", Applied Physics Letters, 105: 021102, (2014). DOI: 10.1063/1.4890521

[13] Ye, Q., Liu, Y., Lin, H., Li, M., Yang, H., "Multi-band metamaterial absorber made of multi-gap SRRs structure", Applied Physics A Materials Science & Processing, 107: 155–160, (2012). DOI: 10.1007/s00339-012-6796-7

[14] He, Y., Wu, Q., Yan, S., "Multi-band terahertz absorber at 0.1–1 THz frequency based on ultra-thin metamaterial", Plasmonics, 14: 1303–1310, (2019). DOI: 10.1007/s11468-019-00936-7

[15] Sood, D., Tripathi, C.C., "Quad band electric field-driven LC resonator based polarisation-insensitive metamaterial absorber", IET Microwaves, Antennas & Propagation, 12(4): 588–594, (2017). DOI: 10.1049/iet-map.2017.0908

[16] Huang, X., Lu, C., Rong, C., Hu, Z., Liu, M., "Multiband ultrathin polarization-insensitive terahertz perfect absorbers with complementary metamaterial and resonator based on high-order electric and magnetic resonances", IEEE Photonics Journal, 10, 6: 4600811, (2018). DOI: 10.1109/JPHOT.2018.2878455

[17] Padilla, W.J., Taylor, A. J., Highstrete, C., Lee, M., Averitt, R.D., "Dynamical electric and magnetic metamaterial response at terahertz frequencies", Physical Review Letters, 96: 107401, (2006). DOI: 10.1103/PhysRevLett.96.107401

[18] Chen, H.-T., Padilla, W.J., Zide, J.M.O., Gossard, A.C., Taylor, A.J., Averitt, R.D., "Active terahertz metamaterial devices", Nature, 444: 597–600, (2006). DOI: 10.1038/nature05343

[19] Ricci, M.C., Xu, H., Prozorov, R., Zhuravel, A.P., Ustinov, A.V., Anlage, S.M., "Tunability of superconducting metamaterials", IEEE Transactions on Applied Superconductivity, 17(2): 918–921, (2007). DOI: 10.1109/TASC.2007.898535

[20] Fedotov, V.A., Tsiatmas, A., Shi, J.H., Buckingham, R., Groot, P. de, Chen, Y., Wang, S., Zheludev, N.I., "Temperature control of Fano resonances and transmission in superconducting metamaterials", Optics Express, 18(9): 9015–9019, (2010). DOI: 10.1364/OE.18.009015

[21] Jin, B.B., Zhang, C., Engelbrecht, S., Pimenov, A., Wu, J., Xu, Q., Cao, C., Chen, J., Xu, W., Kang, L., Wu, P., "Low loss and magnetic field tunable superconducting terahertz metamaterial", Optics Express, 18(16): 17504–17509, (2010). DOI: 10.1364/OE.18.017504

[22] Singh, R., Xiong, J., Azad, A.K., Yang, H., Trugman, S.A., Jia, Q.X., Taylor, A.J., Chen, H.T., "Optical tuning and ultrafast dynamics of high-temperature superconducting terahertz metamaterials", Nanophotonics, 1: 117–123, (2012). DOI: 10.1515/nanoph-2012-0007

[23] Srivastava, Y.K., Manjappa, M., Cong, L., Krishnamoorthy, H.N.S., Savinov, V., Pitchappa, P., Singh, R., "A superconducting dual-channel photonic switch", Advanced Materials, 30: 1801257, (2018). DOI: 10.1002/adma.201801257

[24] Zhao, J., Cheng, Q., Chen, J., Qi, M.Q., Jiang, W.X., Cui, T.J., "A tunable metamaterial absorber using varactor diodes", New Journal of Physics, 15: 043049, (2013). DOI:10.1088/1367-2630/15/4/043049

[25] Yuan, H., Zhu, B.O., Yeng, F., "A frequency and bandwidth tunable metamaterial absorber in X-band", Journal of Applied Physics, 117: 173103, (2015). DOI: 10.1063/1.4919753

[26] Hu, F., Qian, Y., Li, Z., Niu, J., Nie, K., Xiong, X., Zhang, W., Peng, Z., "Design of a tunable terahertz narrowband metamaterial absorber based on an electrostatically actuated MEMS cantilever and split ring resonator array", Journal of Optics, 15: 055101, (2013). DOI: 10.1088/2040-8978/15/5/055101

[27] Yao, G., Ling, F., Yue, J., Luo, C., Ji, J., Yao, J., "Dual-band tunable perfect metamaterial absorber in the THz range", Optics Express, 24(2): 1518–1527, (2016). DOI: 10.1364/OE.24.001518

[28] Mulla, B., Sabah, C., "Improvement of multiband absorption with different technics (graphene, ITO, and hole) for metamaterial absorber at optical frequencies", Journal of Nanophotonics, 12(4): 046017, (2018). DOI: 10.1117/1.JNP.12.046017

[29] Zhou, Q., Liu, P., Bian, L.-A., Cai, X., Liu, H., "Multi-band terahertz absorber exploiting graphene metamaterial", Optical Materials Express, 8(9): 2928–2940, (2018). DOI: 10.1364/OME.8.002928

[30] Liu, C., Qi, L., Zhang, X., "Broadband graphene-based metamaterial absorbers", AIP Advances, 8: 015301, (2018). DOI: 10.1063/1.4998321

[31] Xu, Z., Wu, D., Liu, Y., Liu, C., Yu, Z., Yu, L., Ye, H., "Design of a tunable ultra-broadband terahertz absorber based on multiple layers of graphene ribbons", Nanoscale Research Letters, 13: 143, (2018). DOI: 10.1186/s11671-018-2552-z

[32] Lin, H., Sturmberg, B.C.P., Lin, K.-T., Yang, Y., Zheng, X., Chong, T.K., Sterke, C.M., Jia, B., "A 90-nm-thick graphene metamaterial for strong and extremely broadband absorption of unpolarized light", Nature Photonics, 13: 270–276, (2019). DOI: 10.10138/s41566-019-0389-3.

[33] Ling, K., Yoo, M., Su, W., Kim, K., Cook, B., Tentzeris, M.M., Lim, S., "Microfluidic tunable inkjet-printed metamaterial absorber on paper", Optics Express, 23: 110–120, (2015). DOI: 10.1364/OE.23.000110

[34] Shrekenhamer, D., Chen, W.C., Padilla, W.J., "Liquid crystal tunable metamaterial absorber", Physical Review Letters ,110(17): 177403, (2013). DOI: 10.1103/PhysRevLett.110.177403

[35] Isic, G., Vasic, B., Zografopoulos, D.C., Beccherelli, R., Gajic, R., "Electrically tunable critically coupled terahertz metamaterial absorber based on nematic liquid crystals", Physical Review Applied, 3: 064007, (2015). DOI: 10.1103/PhysRevApplied.3.064007

[36] Luu, D.H., Dung, N.V., Hai, P., Giang, T.T., Lam, V.D., "Switchable and tunable metamaterial absorber in THz frequencies", Journal of Science: Advanced Materials and Devices, 1: 65–68, (2016). DOI: 10.1016/j.jsamd.2016.04.002

[37] Bian, Y., Wu, C., Li, H., Zhai, J., "A tunable metamaterial dependent on electric field at terahertz with barium strontium titanate thin film", Applied Physics Letters, 104: 042906, (2014). DOI: 10.1063/1.4863669

[38] Song, Z.Y., Wang, K., Li, J.W., Liu, Q.H., "Broadband tunable terahertz absorber based on vanadium dioxide metamaterials", Optics Express, 26(6): 7148–7154, (2018). DOI: 10.1364/OE.26.007148

[39] Li, D., Huang, H., Xia, H., Zengb, J., Li, H., Xie, D., "Temperature-dependent tunable terahertz metamaterial absorber for the application of light modulator", Results in Physics, 11: 659–664, (2018). DOI: 10.1016/j.rinp.2018.10.014

[40] Wang, B.-X., Wang, G. Z., "Temperature tunable metamaterial absorber at THz frequencies", Journal of Materials Science: Materials in Electronics, 28: 8487–8493, (2017). DOI: 10.1007/s10854-017-6570-x

[41] Zou, H., Cheng, Y., "Design of a six-band terahertz metamaterial absorber for temperature sensing application", Optical Materials , 88: 674–679, (2019). DOI: 10.1016/j.optmat.2019.01.002

[42] Appasani, B., "An octaband temperature tunable terahertz metamaterial absorber using tapered triangular structures", Progress in Electromagnetics Research Letters, 95: 9–16, (2021). DOI: 10.2528/PIERL20101501

[43] Cunningham, R.W., Gruber, J.B., "Intrinsic concentration and heavy-hole mass in InSb", Journal of Applied Physics, 41(4): 1804–1809, (1970). DOI: 10.1063/1.1659107

[44] Cong, L., Tan, S., Yahiaoui, R., Yan, F., Zhang, W., Singh, R., "Experimental demonstration of ultrasensitive sensing with terahertz metamaterial absorbers: A comparison with the metasurfaces", Applied Physics Letters, 106: 031107, (2015). DOI: 10.1063/1.4906109

[45] Huang, X., He, W., Yang, F., Ran, J., Yang, Q., Xie, S., "Thermally tunable metamaterial absorber based on strontium titanate in the terahertz regime", Optical Materials Express, 9(3): 1377–1385, (2019). DOI: 10.1364/OME.9.001377

[46] Li, W., Kuang, D., Fan, F., Chang, S., Lin, L., "Subwavelength B-shaped metallic hole array terahertz filter with InSb bar as thermally tunable structure", Applied Optics, 51(29): 7098–7102, (2012). DOI: 10.1364/AO.51.007098

[47] Appasani, B., "Temperature tunable seven band terahertz metamaterial absorber using slotted flower–shaped resonator on an InSb substrate", Plasmonics, (2021). DOI: 10.1007/s11468-020-01329-x